BOLETÍN DE LA SOCIEDAD ESPAÑOLA DE CERÁMICA Y VIDRIO XXX (2021) XXX–XXX

BOLETIN DE LA SOCIEDAD ESPAÑOLA DE
Cerámica y Vidrio
www.elsevier.es/bsecv

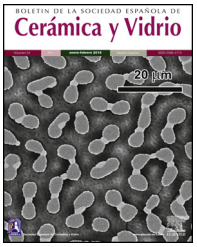

Original article

Effect of Sr, Mg and Fe substitution on the physico-chemical and biological properties of Si–Ca–P multilayer scaffolds

Nayarit A. Mata[a,*], *Marcela Arango-Ospina*[b], *Pablo Velasquez*[a], *Angel Murciano*[c], *Piedad N. De Aza*[a], *Aldo R. Boccaccini*[b]

[a] *Institute of Bioengineering, Miguel Hernandez University, Avda. Universidad s/n, 03202 Elche, Spain*
[b] *Institute of Biomaterials, University of Erlangen-Nuremberg, Cauerstr. 6, 91058 Erlangen, Germany*
[c] *Department of Materials, Optical and Electronic Technology, Miguel Hernandez University, Avda. Universidad s/n, 03202 Elche, Spain*

ARTICLE INFO

Article history:
Received 7 October 2021
Accepted 15 November 2021
Available online xxx

Keywords:
Bioceramics
Sol–gel
Scaffolds
Ion doping

ABSTRACT

In this work, a new combination of ceramic materials is proposed for bone tissue engineering applications. Multilayer scaffolds consisting of a core composed mainly of calcium pyrophosphate and external coatings of silica and calcium doped with Fe^{3+}, Sr^{2+} and Mg^{2+} were prepared. To study the influence of the arrangement of dopant ions in the external coatings, two different scaffolds were developed: scaffolds 3J consisting of a single external coating with 9 mol% of Fe^{3+}, Sr^{2+} and Mg^{2+} ions; and scaffolds 3S comprising three external coatings, each containing 3 mol% of Fe^{3+}, Sr^{2+} and Mg^{2+} ions. Scaffolds were physico-chemically characterized and evaluated for *in vitro* bioactivity and cellular response in the presence of MG-63 cells. The results showed that the core scaffold displayed no *in vitro* bioactivity or good cellular response, but served as a support for the external coatings given its mechanical resistance. The cell viability of scaffolds 3J and 3S increased more than 100% in relation to the core, and also improved cell proliferation and adhesion resulting in a dense layer of cells that covered the scaffolds' entire surface. The arrangement of ions in the external coatings did not influence the cellular response, but determined the bioactivity rate.

* *Corresponding author.*
E-mail address: nmata@umh.es (N.A. Mata).
https://doi.org/10.1016/j.bsecv.2021.11.005

Please cite this article in press as: N.A. Mata, et al., Effect of Sr, Mg and Fe substitution on the physico-chemical and biological properties of Si—Ca—P multilayer scaffolds, Bol. Soc. Esp. Cerám. Vidr. (2021), https://doi.org/10.1016/j.bsecv.2021.11.005

Efecto de la sustitución de Sr, Mg y Fe en las propiedades físico-químicas y biológicas de andamios multicapa de Si-Ca-P

Palabras clave:
Biocerámicas
Sol-gel
Andamios
Dopaje iónico

RESUMEN

En este trabajo se propone una nueva combinación de materiales cerámicos para aplicaciones en ingeniería de tejido óseo. Se prepararon andamios multicapa formados por un núcleo principalmente de pirofosfato cálcico y recubrimientos externos de sílice y calcio dopados con Fe^{3+}, Sr^{2+} y Mg^{2+}. Para estudiar la influencia de la disposición de los iones dopantes en los recubrimientos externos, se desarrollaron dos andamios diferentes: andamios 3J con un recubrimiento externo con 9 mol% de Fe^{3+}, Sr^{2+} y Mg^{2+}; y andamios 3S con tres recubrimientos externos, cada uno con 3 mol% de Fe^{3+}, Sr^{2+} y Mg^{2+}. Posteriormente, se realizó caracterización fisicoquímica, se evaluó su bioactividad *in vitro* y respuesta celular en presencia de células MG-63. Los resultados mostraron que el núcleo del andamio no presentaba bioactividad ni buena respuesta celular, pero servía de soporte para los recubrimientos externos debido a la resistencia mecánica. La viabilidad celular de los andamios 3J y 3S aumentó en más de 100% respecto al núcleo y mejoró la proliferación y adhesión celular, dando lugar a una densa capa de células en la superficie de los andamios. La disposición de los iones en los recubrimientos externos no influyó en la respuesta celular, pero determinó la tasa de bioactividad.

Introduction

Tissue engineering is a multidisciplinary field that uses engineering tools and health science to solve tissue degradation and regeneration problems [1]. This field involves three indispensable components: (i) cells; (ii) scaffolds and (iii) biological factors [2–5]. Scaffolds play an important role because they act as the physical matrix where biological entities are deposited to promote the integration and/or restoration of damaged tissue. For this reason, the choice of the scaffold's biomaterial must be in accordance with the tissue type to be treated.

In recent years, bone has become one of the most replaced tissues, mainly by the increase in skeletal system trauma due to motor vehicle use and degenerative diseases as a result of increased life expectancy [6,7]. The selection of a biomaterial that mimics bone is complicated because of the hierarchical structure and the biological processes that occur in this kind of tissue [8,9].

Ceramic materials are an excellent choice for restoring hard tissues for their similarity to the bone mineral component [10–12]. Although ceramic materials are able to chemically imitate bone and provide biocompatibility, a scaffold with a single chemical composition is not sufficient to fulfill all the requirements that a scaffold must meet: good mechanical strength, porous structure, osteoconductivity, osteoinductivity, biodegradability, among others [8,13,14]. For this reason, previous studies have proposed creating multilayer scaffolds consisting of coatings with different chemical compositions to provide several characteristics [15–18].

The present research work proposes creating a core formed by a chemical composition that confers mechanical resistance, and it is subsequently coated by bioactive compositions doped with ions like Fe^{3+}, Sr^{2+} and Mg^{2+}. Naturally, these ions are found in bone and participate in different processes, which is why these ions have been widely incorporated into various ceramic and glass materials [19–22]. Strontium behaves similarly to calcium, stimulates osteoblast activity and restricts osteoclast differentiation [19,23]. Magnesium stimulates new bone formation and increases cell adhesion [24]. Iron participates in tissue growth and blood vessel formation [19]. These ions have been previously incorporated individually into external coatings of multilayer scaffolds to present apatite precipitates during *in vitro* bioactivity evaluations [16–18].

Hence this research work aims to integrate these three ions (in the ideal ionic concentration obtained in the previous studies) into a unique scaffold to enhance the benefits of each ion. Multilayer scaffolds were prepared with the same calcium phosphate core but were coated by external coatings of mainly calcium silicate doped with Fe^{3+}, Sr^{2+} and Mg^{2+} in two different configurations. The first configuration included a single external coating with 3 mol% of each ion (Fe^{3+}, Sr^{2+} and Mg^{2+}); *i.e.* 9 mol% doping in relation to the total calcium moles. In the second configuration, coatings of 3 mol% of each ion were incorporated into three different layers; *i.e.* the first was a iron-doped coating, the next was a strontium-doped coating, and the most external was a magnesium-doped coating. Scaffolds were physico-chemically characterized. Subsequently, the *in vitro* bioactivity and behavior in cell culture were evaluated by indirect (extracts of material powder) and direct (scaffold) assays.

Materials and methods

Scaffold preparation

Scaffolds were prepared by sol-gel and the polymer replica method. The reagents used to prepare the sol-gel solution were tetraethyl orthosilicate (TEOS – $Si(OC_2H_5)_4$) as a source

Please cite this article in press as: N.A. Mata, et al., Effect of Sr, Mg and Fe substitution on the physico-chemical and biological properties of Si—Ca—P multilayer scaffolds, Bol. Soc. Esp. Cerám. Vidr. (2021), https://doi.org/10.1016/j.bsecv.2021.11.005

Table 1 – Formulations of ceramics (mol%).

Formulation	SiO_2	P_2O_5	CaO	Li_2O	SrO	MgO	Fe_2O_3
Formulation 1	1	25	68	6	–	–	–
Formulation 2	29	3	63		2	2	1
Formulation 3	29	3	67	–	–	–	1
Formulation 4	29	3	66	–	2	–	–
Formulation 5	29	3	66	–	–	2	–

of silicon, triethyl phosphate (TEP – $(C_2H_5)_3PO_4$) as a source of phosphorous, and calcium carbonate as a source of calcium. They were all provided by Sigma–Aldrich. The reagents used to introduce ions into the sol–gel solution were lithium carbonate (Li_2CO_3), strontium carbonate ($SrCO_3$) and magnesium carbonate ($MgCO_3$), all provided by Sigma-Aldrich, and ferrous sulfate heptahydrate ($FeSO_4{\cdot}7H_2O$) supplied by Merck. Solutions were prepared in a medium with distilled water, 37% hydrochloride acid (HCl – Ensure) and 97% ethanol (C_2H_5OH – Guimana). Table 1 shows all formulations made by this method. The employed polymer template was a polyurethane sponge with 20 pores per inch, 12.7 mm diameter and 10 mm high.

Multilayer scaffolds were constituted by a core and external layers. Core composition was SiO_2—$25P_2O_5$—68CaO—$6Li_2O$ mol% (Formulation 1) and the composition of external coatings was $29SiO_2$—$3P_2O_5$—68CaO mol%. To introduce the dopant, the latter composition was modified to obtain formulations 2–5. Based on these formulations, two different configurations were selected for the scaffolds.

Core

The solution of formulation 1 was prepared with 11.4 ml of TEP, 20 ml of distilled water, 5 ml of ethanol, 0.36 ml of TEOS, 10 ml of HCl, 0.5 g of Li_2CO_3 and 8.38 g of $CaCO_3$. Before adding carbonates, the solution was stirred for 30 min. Drops of HCl were added to keep the solution's pH between 2 and 3. The solutions with all the reagents were heated for 30 min at 100 °C with stirring. After this time, the solution formed an oily phase capable of covering the polymeric sponge. The polyurethane templates where immersed into the solution 30 times. After each immersion, sponges were centrifuged at 500 rpm and oven-dried at 140 °C to ensure the formation of a coating. Finally, the green bodies were sintered at 950 °C at a heating rate of 18 °C/h and maintained for 8 h.

Scaffold configuration 1 (scaffold 3J)

The configuration 1 (labeled 3J) consisted of a core scaffold coated with Formulation 2. In this formulation, 9% of the original total calcium moles were substituted by 3% of each doping ion (Fe^{+2}, Mg^{+2} and Sr^{+2}). The solution was prepared with 11.01 ml of TEOS, 20 ml of distilled water, 5 ml of ethanol, 1.64 ml of TEP, 10 ml of HCl, 0.5 g of $SrCO_3$, 0.29 g of $MgCO_3$, 0.94 g of $FeSO_4.7H_2O$ and 10.3 g of $CaCO_3$. Core scaffolds were immersed in this solution 6 times. After each immersion, samples were centrifuged and oven-dried. Finally, samples were sintered at 950 °C at a heating rate of 92.5 °C/h and maintained for 3 h.

Scaffold configuration 2 (scaffold 3S)

The configuration 2 (labeled 3S) consisted of a core scaffold coated with Formulations 3, 4 and 5. In all these formulations, 3% of the total calcium moles were substituted by Fe^{+2}, Sr^{+2} and Mg^{+2}, respectively. The first coating layer was doped with iron. Subsequently, it was coated with the strontium-doped coating and finally by the magnesium-doped coating. The amounts of ions were selected so that the ion concentrations were the same. Three solutions were prepared with 11.01 ml of TEOS, 20 ml of distilled water, 5 ml of ethanol, 1.64 ml of TEP, 10 ml of HCl, 11 g $CaCO_3$, and each solution with 0.5 g of $SrCO_3$, 0.29 g of $MgCO_3$ and 0.94 g of $FeSO_4{\cdot}7H_2O$, respectively. For each layer, the sample was immersed 6 times in solution. Before coating with the next layer, the sample was sintered at 950 °C at a heating rate of 92.5 °C/h and maintained for 3 h.

Scaffolds characterization

Mineralogical characterization by X-ray diffraction

The chemical and mineralogical characterizations of scaffolds were evaluated by X-ray diffraction (XRD). A Bruker AXR D8 Advance equipment was used with a secondary graphite monochromator and Cu-Kα radiation (1.5418740 Å). The X-ray tube operated at 40 kV and 30 mA with 0.02 steps by counting 8s per step. Data were collected between 20 and 40 degrees (2θ). The software Match!, version 3.9.0.158, was used for the analysis, and diffractograms were compared to the Crystallography Open Database (COD).

Microstructural characterization

The microstructure and morphology of scaffolds were studied by Scanning Electron Microscopy with Energy Dispersive X-ray (SEM-EDX). A Hitachi S-3500N with INCA system by Oxford Instruments Analytical was used. Samples were gold- and palladium-coated prior to evaluation.

Physical characterization

Ten scaffolds of each type were employed to study physical properties (8.5 mm diameter and 7.0 mm high). Scaffolds' porosity was measured by a pycnometer according to Arquimedes' principle. Scaffolds' maximum compressive strength was measured by a Simple Test Stand (NEURTEK instruments SVL-1000N). Force was applied to the scaffolds surface until total failure and the maximum force was recorded with a digital force gauge dst/dsv SERIES. Maximum compressive strength was calculated according to the following equation:

$$\sigma_m = \frac{F_m}{A}$$

where σ_m (MPa) is maximum compressive strength, F_m (N) is maximum force and A (mm^2) is the area perpendicular to the applied force.

In vitro bioactivity evaluation

Scaffolds' *in vitro* bioactivity was evaluated by the ability to precipitate apatite on the surface when immersed in simulated body fluid (SBF). Scaffolds 3J and 3S were soaked in SBF prepared according to Standard ISO/FDIS 23317:2017 for

Please cite this article in press as: N.A. Mata, et al., Effect of Sr, Mg and Fe substitution on the physico-chemical and biological properties of Si—Ca—P multilayer scaffolds, Bol. Soc. Esp. Cerám. Vidr. (2021), https://doi.org/10.1016/j.bsecv.2021.11.005

ceramics and powder samples during different periods. The ceramic scaffolds (8.5 mm diameter and 7.0 mm high) were immersed in 50 ml of SBF and kept for 3, 14 and 21 days in water bath at 37 °C.

After each period, a sample was evaluated by SEM-EDX and the SBF aliquot was assessed by inductively coupled plasma optical emission spectrometry (ICP-EOS). In the last test, a Thermo iCAP 6500 DUO equipment was used to analyze the ionic element concentration in the resulting SBF. The *in vitro* bioactivity of the scaffolds' core has been previously studied [18].

Indirect cell culture

Ion release

In order to study the influence of the ions released by materials with cells, the powder from each scaffold was put into contact with cell culture medium (CCM) before seeding cells. The core and scaffolds 3J and 3S were ground using an agate mortar and sterilized at 160 °C for 2 h. Powders at 10 mg/ml and 100 mg/ml were brought into contact with Dulbecco's modified Eagle Medium (DMEM – Gibco) supplemented with 10% Fetal Bovine Serum (FBS – Corning) and 1% penicillin/streptomycin (PS – Gibco) in 15 ml falcon tubes for 24 h, and then for 96 h in a shaking incubator at 90 rpm and 37 °C.

Analysis of the released ions

An aliquot of the CCM, which was brought into contact with the powder of each scaffold at both concentrations for 24 h and 96 h, was analyzed by ICP-OES to know which ions were released by each material. The pH of the CCM was measured with a Mettler Toledo instrument (FiveEasy Plus).

Cell culture

Cell assays were performed using osteosarcoma cell line MG-63. Cells were cultured in 75 cm^2 culture flasks with DMEM supplemented with 10% FBS and 1% PS and incubated at 37 °C in a humidified atmosphere with 5% CO_2 and in a 95% air environment. Every 2 days, cells were passaged when 80% confluency had been reached. During the passage, the medium was removed to eliminate non-adherent cells, washed with Dulbecco's Phosphate Buffered Saline (DPBS – Gibco) and, finally, cells were collected using trypsin-EDTA (Gibco). Cells were counted using trypan blue and a hemocytometer. One day before the indirect assay, cells were seeded in 24-well plates at a concentration of 100,000 cells/ml. After 24 h and 96 h, the falcon tubes with the CCM and powders were centrifuged at 2000 rpm for 5 min. Then the CCM supernatants were transferred to the 24-well plates with the previously seeded cells and incubated at 37 °C in a humidified atmosphere with 5% CO_2. The control for this assay was cells brought into contact with the non-conditioned CCM.

Cell viability

After incubating for 1 day (D1) and 3 days (D3), cell viability was studied by the cell-counting kit containing water-soluble tetrazolium salt (WST-8). This salt reduces cell dehydrogenase, which results in a water-soluble formazan that is characterized as being yellow-colored and is proportional to the number of viable cells. For this assay, the CCM of each well was transferred to Eppendorf tubes and reserved at incubator conditions during the analysis. Subsequently, 500 μl of a solution containing 1 vol% WST-8 and 99 vol% of the CCM were added to each well. After a 2 h incubation at 37 °C, 100 μl of each well were transferred to a 96-well plate and the absorbance was measured at 450 nm (FLUOstar Omega, BMG LABTECH). The absorbance value of the 1 vol% WST-8 solution was subtracted from all the absorbance values. After a 1-day analysis, the solution was removed from the 24-well plate, washed with DPBS, and the previously reserved CCM was returned to each well to continue the incubation period until day 3, time at which the procedure was repeated.

LDH activity

Lactate dehydrogenase (LDH) activity was studied after 3 days. LDH is an enzyme that is found inside cells and is released when cell membrane damage occurs. LDH activity is used to not only study cytotoxicity, but also to measure the number of cells that remain until the end of the assay by rupturing the membrane so they can be released. The LDH enzyme catalyzes the conversion of lactate and pyruvate by reducing NAD to NADH, which is then detected by absorbance. For this assay, the CCM was removed, washed with DPBS and 1 ml of lysis buffer (containing 0.1 wt% Triton X, 20 mM TRIS, 1 mM $MgCl_2$ and 0.1 mM $ZnCl_2$) was added to each well and left for 30 min. Subsequently, the lysis buffer was transferred from each well to Eppendorf tubes and centrifuged at 2000 rpm for 5 min. 140 μl of the supernatant from each Eppendorf tube and 60 μl of the LDH solution were added (containing 20 μl of the LDH assay substrate solution, 20 μl of the LDH assay dye and 20 μl of the LDH assay cofactor solution) to a 48-well plate. Finally, the well plate was incubated in the dark for 30 min, the reaction was stopped with 300 μl of HCl 1 M, and the absorbance was measured at 490 nm.

Direct cell culture

Sample preparation and cell seeding.

The core and scaffolds 3J and 3S were sterilized at 160 °C for 2 h. Samples were pre-conditioned to wet the scaffold surface and prepare it for cell attachment. For this purpose, scaffolds were placed inside a 24-well plate together with 1.5 ml of the CCM and were incubated for 30 min at 37 °C and 5% CO_2. After the pre-conditioning time, the CCM was removed and seeding was performed with the previously cultured MG-63 cells in a drop-wise manner by placing a drop of 25 μl containing 50,000 cells on the surface of each scaffold to be incubated for 30 min at 37 °C and 5% CO_2. This procedure was repeated once again. After the last 30-minute period, the CCM was added to each well. Samples were incubated for 1, 3, 7, 14 and 21 days. The CCM was refreshed every 2 days.

Cell viability

The viability of the cells in each scaffold was studied by WST-8. After each assay time (1, 3, 7, 14 and 21 days), the CCM was removed and scaffolds were transferred to a new 24-well plate to avoid considering the cells at the bottom of wells. Subsequently, 1.5 ml of a solution containing 1 vol% WST-8 and 99 vol% CCM was added to each well and incubated for 3 h at 37 °C and 5% CO_2. Afterward, 100 μl of each well were

Please cite this article in press as: N.A. Mata, et al., Effect of Sr, Mg and Fe substitution on the physico-chemical and biological properties of Si—Ca—P multilayer scaffolds, Bol. Soc. Esp. Cerám. Vidr. (2021), https://doi.org/10.1016/j.bsecv.2021.11.005

transferred to a 96-well plate and absorbance was measured at 450 nm.

LDH activity

After 7, 14 and 21 days, scaffolds were transferred to a new 24-well plate and cells were lysed with 1.5 ml of lysis buffer to each sample. After 30 min, the procedure described above for the indirect assay was repeated.

Cell morphology evaluation

The evaluation of cell morphology, adhesion and proliferation on scaffolds' surface was performed by fluorescence staining and SEM. Fluorescence staining was carried out using rhodamine phalloidin red staining to observe the cytoplasm and DAPI (4′,6-diamidino-2′-phenylindole, dihydrochloride) blue staining to view cell nuclei. Images were obtained with a fluorescence microscope (Axio Scope A.1, Carl Zeiss).

For SEM, the cells on the surface of samples were fixed with two solutions for 1 h, the first containing glutaraldehyde and sodium cacodylate and the second with glutaraldehyde, sodium cacodylate and paraformaldehyde. Next a dehydration process was carried out with a series of alcohols from 30% to 99.5% ethanol, and each alcohol was brought into contact with the samples for 30 min. Finally, samples were dried at the critical point (Leica EM CPD300) and viewed by SEM (Auriga CrossBeam, Carl Zeiss).

Statistics

The results are shown as the mean values and standard deviation. The significant difference between values was calculated with the Origin software and the one-way analysis of variance ANOVA by a Tukey test. The significance level is given by a p-value of $p < 0.05 = ^*$.

Results

Scaffold characterization

Ceramic scaffolds obtained after the sintering process maintained the cylindrical shape with 8.5 mm diameter and 7.0 mm high approximately, as well as a weight of (0.35 ± 0.10) g.

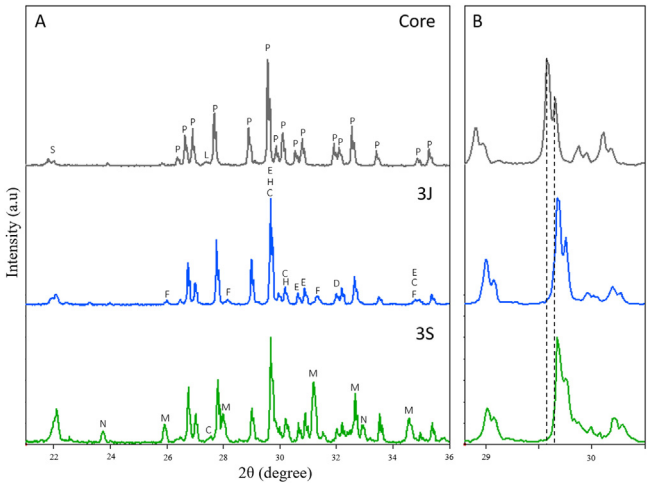

Fig. 1 – (A) The XRD patterns of the core and scaffolds 3J and 3S. (B) Details of the principal peaks. P: $Ca_2P_2O_7$, S: SiO_2, L: $Li(PO_3)$, H: $Mg_2P_2O_7$, F: $Ca_{9.333}Fe_{1.167}(PO_4)_7$, M: $Ca_{10.115}Mg_{0.385}(PO_4)_7$, E: $Ca_{0.1}Fe_{0.6}Mg_{1.3}(SiO_3)_2$, C: $Ca_{0.90}Mg_{0.71}Fe_{0.25}(SiO_3)_2$, D: $Ca_{1.65}Sr_{0.35}(SiO_4)$, N: $CaLi(PO_4)$.

The mineralogical characterization carried out by XRD to study the scaffolds crystalline phases is shown in Fig. 1. In this figure, it is observed that the core is formed mainly by calcium pyrophosphate ($Ca_2P_2O_7$ – COD 96-100-1557) and by a minority of silicon dioxide (SiO_2 – COD 96-101-0939) and $Li(PO_3)$ (COD 96-210-7073). Additionally, the principal peaks of $Ca_2P_2O_7$ phase reported at 2θ 29.57° and 29.65° were slightly shifted to 2θ 29.60° and 29.68°.

Subsequently, the diffractograms of scaffolds 3J and 3S were analized. The following changes can be distinguished in the diffractograms:

(i) The diffractograms of scaffolds 3J and 3S are shifted to the right in relation to the core, as shown in detail in Fig. 1(B). The main peaks shifted to 2θ 29.68° and 29.76°. This means that ions entered the crystalline structure of calcium pyrophosphate. Specifically, phase $Mg_2P_2O_7$ (COD 96-201-7953) was identified. At these peaks

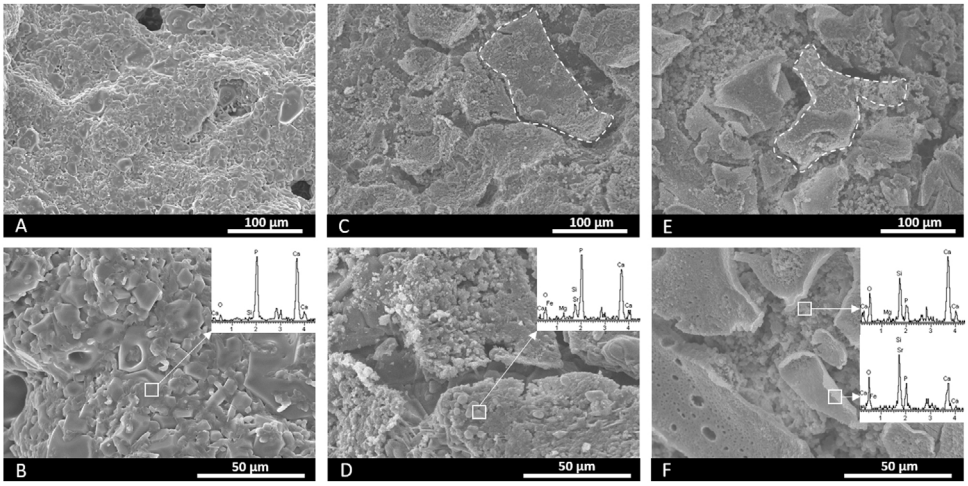

Fig. 2 – SEM-EDX images of the core (A, B), and scaffolds 3J (C, D) and 3S (E, F).

Please cite this article in press as: N.A. Mata, et al., Effect of Sr, Mg and Fe substitution on the physico-chemical and biological properties of Si—Ca—P multilayer scaffolds, Bol. Soc. Esp. Cerám. Vidr. (2021), https://doi.org/10.1016/j.bsecv.2021.11.005

new phases were identified and corresponded to non-stoichiometric calcium silicate substituted for iron and magnesium ions ($Ca_{0.1}Fe_{0.6}Mg_{1.3}(SiO_3)_2$ – COD 96-152-9618 and $Ca_{0.90}Mg_{0.71}Fe_{0.25}(SiO_3)_2$ – COD 96-153-0360).

(ii) The calcium pyrophosphate phase peaks of the core decreased, and new phases appeared that corresponded to tricalcium phosphate (TCP) substituted for iron ($Ca_{9.333}Fe_{1.167}(PO_4)_7$ – COD 96-400-2456, TCP-Fe) and magnesium ($Ca_{10.115}Mg_{0.385}(PO_4)_7$ – COD 96-901-2137, TCP-Mg). In both scaffolds, the two phases were identified but not in the same proportion. In scaffolds 3J, the main phase was the TCP-Fe phase, whereas in scaffolds 3S the TCP-Mg phase was identified.

(iii) The peak corresponding to SiO_2 phase identified at 2θ 22.02° increased, especially in scaffolds 3S.

(iv) A minor strontium silicate phase ($Ca_{1.65}Sr_{0.35}(SiO_4)$ – COD 96-153-5820) was identified in both scaffolds at 2θ 32.90°.

(v) A TCP phase substituted for lithium ($CaLi(PO_4)$ – COD 96-722-2995, TCP-Li) was identified at 2θ 23.63° and 32.89° in scaffolds 3S.

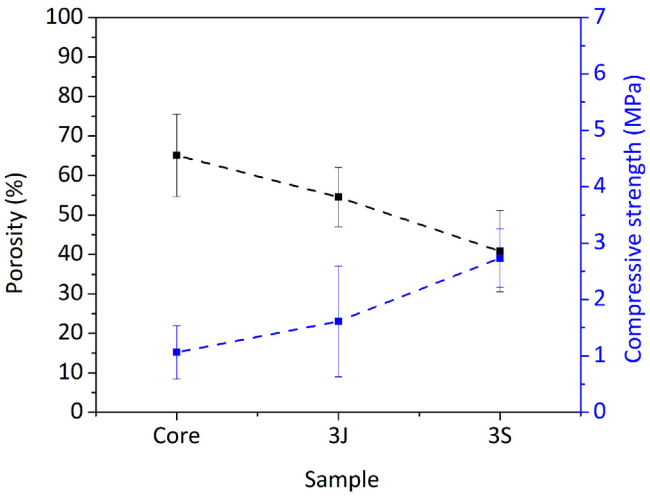

Fig. 3 – Porosity and compressive strength representation of the core and scaffolds 3J and 3S.

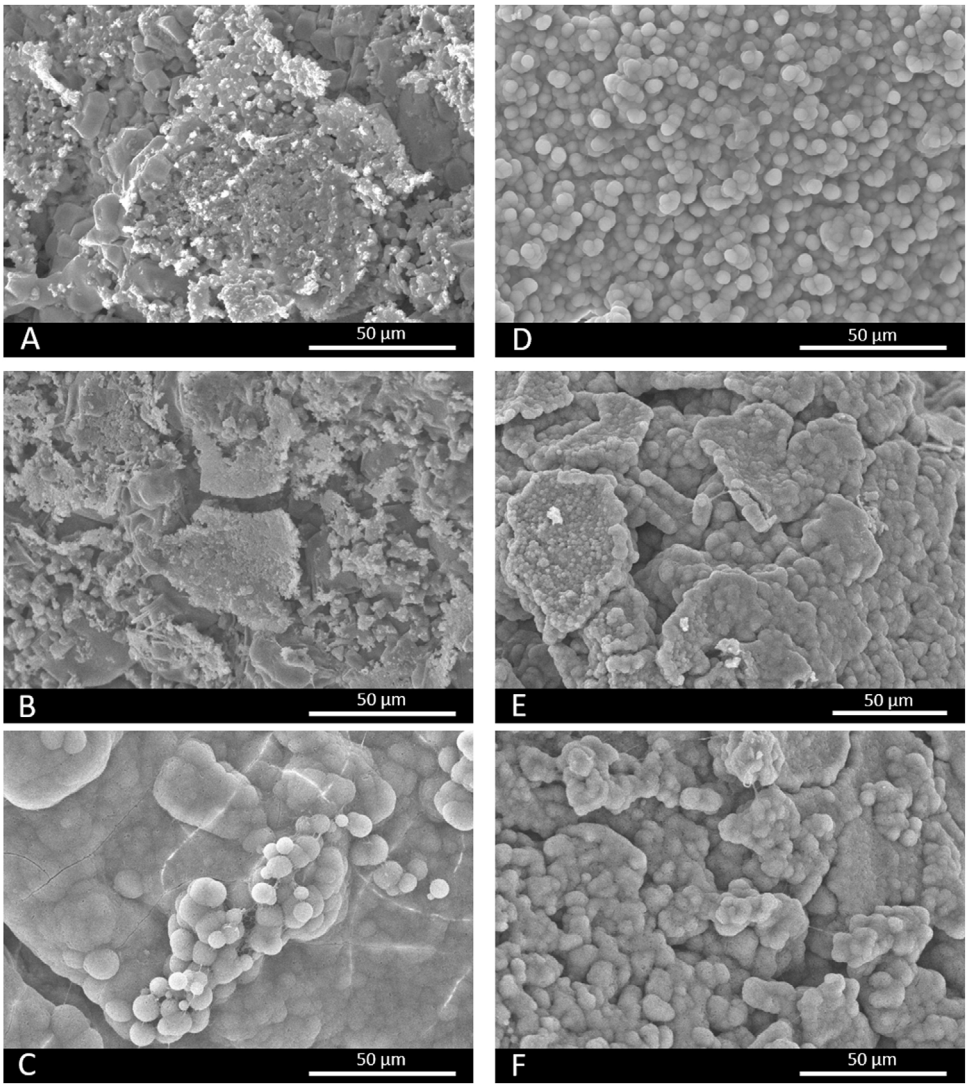

Fig. 4 – SEM images of scaffolds 3J (A-C) and 3S (D-F) after 3, 14 and 21 days of immersion in SBF.

Please cite this article in press as: N.A. Mata, et al., Effect of Sr, Mg and Fe substitution on the physico-chemical and biological properties of Si—Ca—P multilayer scaffolds, Bol. Soc. Esp. Cerám. Vidr. (2021), https://doi.org/10.1016/j.bsecv.2021.11.005

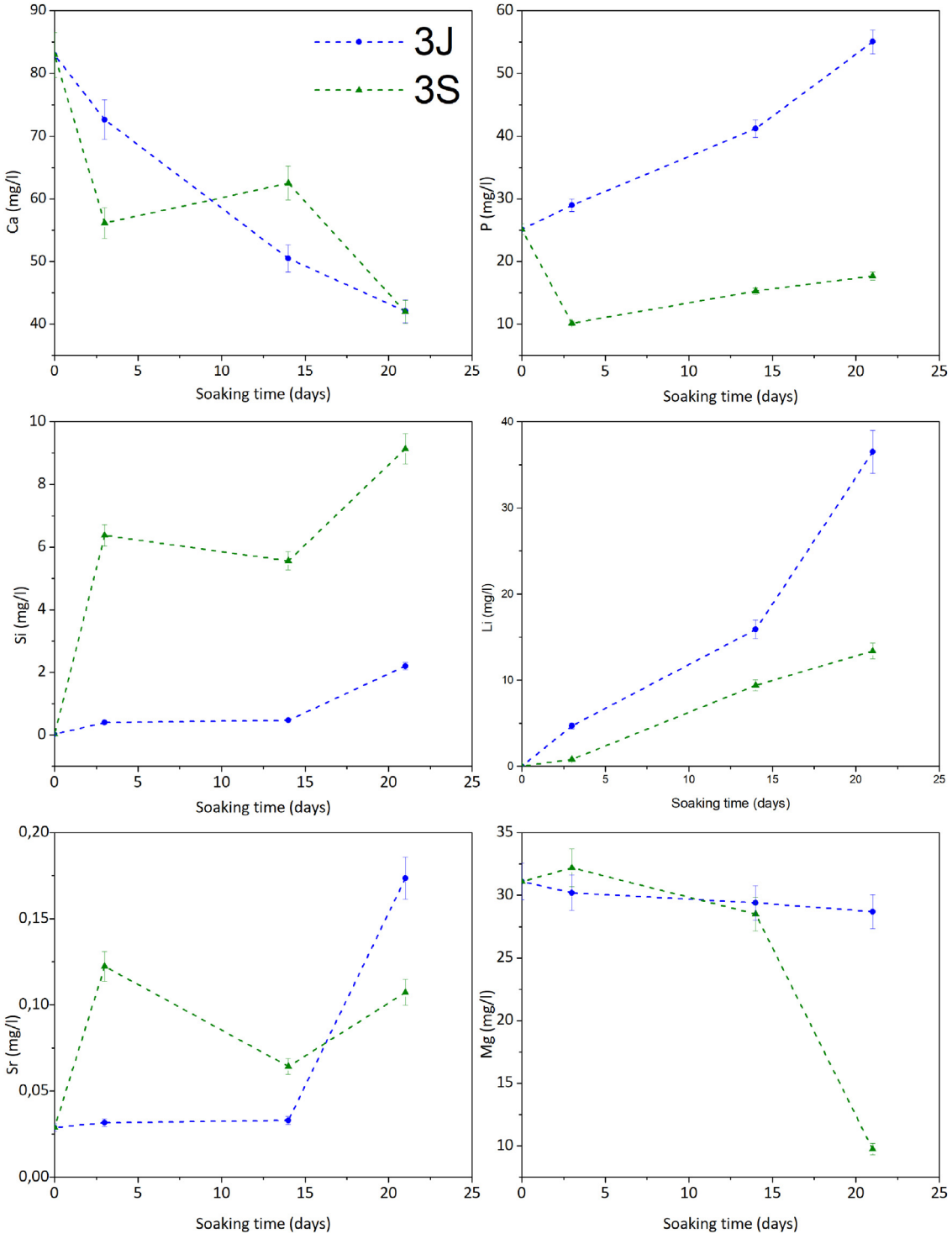

Fig. 5 – Variation in the ionic concentration in SBF after the immersion of scaffolds 3J and 3S at different times.

Fig. 2 (A, B) illustrates the core's microstructure formed by grains of different sizes and shapes. Fig. 2(C–F), which corresponds to the surfaces of scaffolds 3J and 3S, depicts the plates of coatings (marked by dotted lines) over the core. For scaffolds 3J, the core's microstructure lies underneath plates. For scaffold 3S, the previous Sr coating lies beneath the external Mg coating. The EDX analysis on the surface is inserted into the images of each scaffold. This analysis confirmed that the core contained mainly calcium and phosphorus. In addition to calcium and phosphorus, scaffolds 3J contained silicon, strontium, iron and magnesium. In scaffolds 3S, in addition to calcium, phosphorus and silicon, the presence of the dopant ions was detected depending on the surface point.

Fig. 3 shows the scaffolds' physical characteristics, such as compressive strength and porosity. The core's porosity was 65%, which decreased to 40% due to the coatings in scaffolds

Please cite this article in press as: N.A. Mata, et al., Effect of Sr, Mg and Fe substitution on the physico-chemical and biological properties of Si—Ca—P multilayer scaffolds, Bol. Soc. Esp. Cerám. Vidr. (2021), https://doi.org/10.1016/j.bsecv.2021.11.005

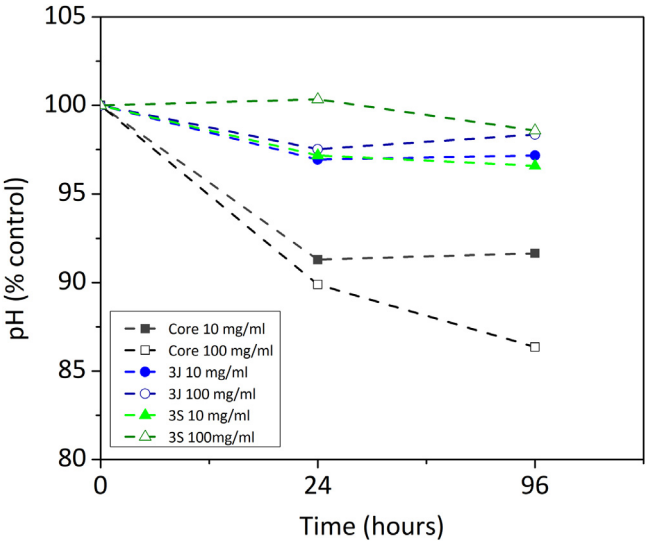

Fig. 6 – Variation in pH in the CCM (pH 8.5) after coming into contact with the core, 3J and 3S powders at 10 mg/ml and 100 mg/ml for 24 h and 96 h.

3S. Mechanical strength rose from (1.00 ± 0.47) MPa in the core to (2.74 ± 0.52) MPa in scaffolds 3S (see Fig. 3).

In vitro bioactivity evaluation

Fig. 4 shows the SEM images of scaffolds 3J and 3S after immersion in SBF. Fig. 4(A, B) depict how scaffolds 3J still have part of the coating after 3 and 14 immersion days. However, after 21 days (Fig. 4C), spherical precipitates were observed on the surface. In contrast, after 3 days the scaffolds 3S showed these precipitates on the surface (Fig. 4D), which remained even up to 21 days (Fig. 4F). The EDX analysis revealed that these precipitates were apatite-like.

Fig. 5 illustrates the study of the ionic interaction between scaffolds 3J/3S and SBF. Scaffolds 3J showed calcium adsorption and phosphorus release during the test, while silicon and strontium started to be released from the beginning of the test with a significant release at 21 days. In contrast, scaffold 3S displayed strong calcium and phosphorus adsorption and the release of silicon and strontium at the beginning of the test. The release of lithium took place in both scaffolds. In relation to magnesium, only scaffold 3S showed adsorption at 21 days. No iron ions were detected.

Indirect cell culture

The indirect cell assay revealed how the ions released by the scaffolds influenced cell behavior. Fig. 6 shows the first parameter herein considered, the variation in pH after 24 h and 96 h of exposing the powder of each scaffold with CCM. The powder of scaffolds 3J and 3S at concentrations of 10 and 100 mg/ml brought about a slight drop in the medium's pH after 96 h, but no more than 3.5%. In contrast, the core powder at a 10 mg/ml and 100 mg/ml concentration lowered the pH by 8.4%, and 13.7%.

The release of ions in the CCM for each material at both concentrations, and after 24 h and 96 h, is shown in Fig. 7. In the core material, at both concentrations, the release of phosphorus, lithium and silicon ions took place. At the 10 mg/ml concentration, the supernatant of the scaffolds 3J showed only silicon release. When the concentration rose to 100 mg/ml, the release of silicon, calcium and strontium became greater. Finally, at the above-mentioned concentrations, only significant silicon release was observed for scaffold 3S.

The viability of the cells incubated with the different conditioned CCMs is shown in Fig. 8. After 1 day (D1), the viability of the cells corresponding to the core's medium, and at both concentrations (10 mg/ml and 100 mg/ml) and times (24 h and 96 h), significantly decreased compared to the control. After 3 days (D3), the viability of the cells in contact with the core's medium at 10 mg/ml and both times increased to values that equaled the control. In contrast, the cells in contact with the core's medium at 100 mg/ml and both times were lower than the control. The viability of the cells in contact with the media of 3J and 3S at both concentrations and times also equaled the viability of the control or was slightly higher, which was the case of the cells in contact with the media of 3J and 3S at 10 mg/ml and both times.

The number of cells after 3 days in each case is shown in Fig. 9. Although a slight decrease in the number of cells was observed in relation to the control, no significant difference appeared.

Direct cell culture

After evaluating the influence of the released ions on cells, the behavior of the cells that came into direct contact with the scaffold was studied. Fig. 10 shows the results of the viability of the cells in contact with the core and scaffolds 3J and 3S. The viability of cells in contact with the core increased over time, with no significant difference from day 1 to day 21. In contrast, the cell viability of scaffolds 3J and 3S increased with time, with a significant difference from day 1. After 14 and 21 days, the viability of the cells in scaffolds 3J and 3S was significantly higher compared to the core. Cell viability after 21 days increased by approximately 110% in scaffold 3J and by 130% in scaffold 3S compared to the core.

Fig. 11 shows the results obtained from analyzing LDH activity. The number of cells in scaffolds 3J and 3S was nearly the same after 7, 14 and 21 days. In contrast, the number of cells in the core significantly decreased after 14 days.

Regarding the visual evaluation of the cells on the scaffolds, Figs. 12 and 13 show images of the surface obtained by fluorescence microscopy and SEM.

Fig. 12 depicts the surface of the core (Fig. 12A, B) and scaffolds 3J (Fig. 12C, D) and 3S (Fig. 12E, F) after 3 and 7 days. Due to staining, cell nuclei are denoted in blue and the cytoskeleton in red. On the core's surface, single round cells were observed, while others formed agglomerates. No difference in cell development appeared between days 3 (Fig. 12A) and 7 (Fig. 12B). With scaffolds 3J (Fig. 12C) and 3S (Fig. 12E), after 3 days a higher number of round-shaped cells were observed on the surface. Some of these cells spread as indicated by the arrow. After 7 days (Fig. 12D, F), cell proliferation was observed due

Please cite this article in press as: N.A. Mata, et al., Effect of Sr, Mg and Fe substitution on the physico-chemical and biological properties of Si—Ca—P multilayer scaffolds, Bol. Soc. Esp. Cerám. Vidr. (2021), https://doi.org/10.1016/j.bsecv.2021.11.005

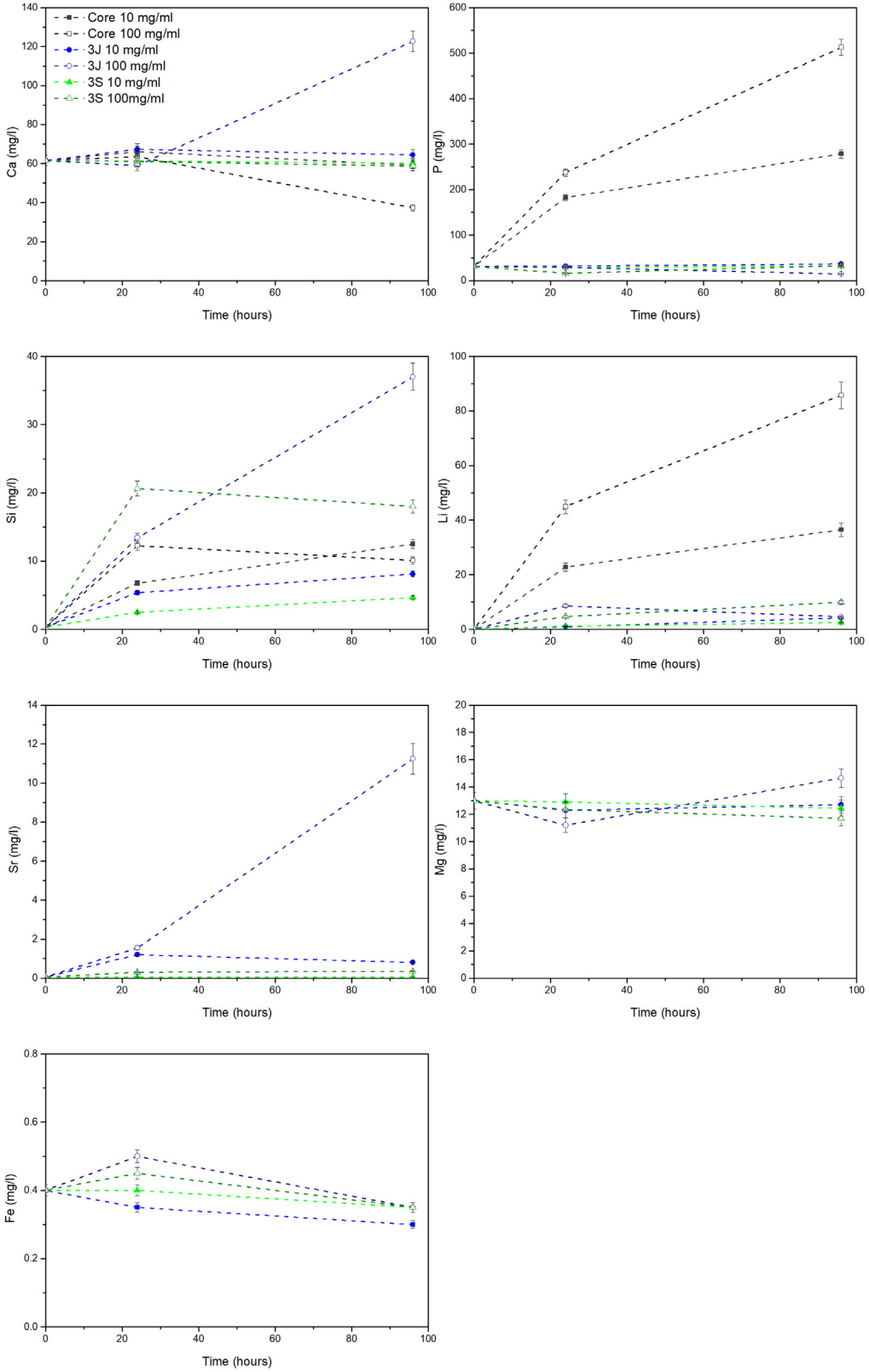

Fig. 7 – Variation of the ionic concentration in the CCM after coming into contact with the core, 3J and 3S powders at 10 mg/ml and 100 mg/ml for 24 h and 96 h.

Please cite this article in press as: N.A. Mata, et al., Effect of Sr, Mg and Fe substitution on the physico-chemical and biological properties of Si—Ca—P multilayer scaffolds, Bol. Soc. Esp. Cerám. Vidr. (2021), https://doi.org/10.1016/j.bsecv.2021.11.005

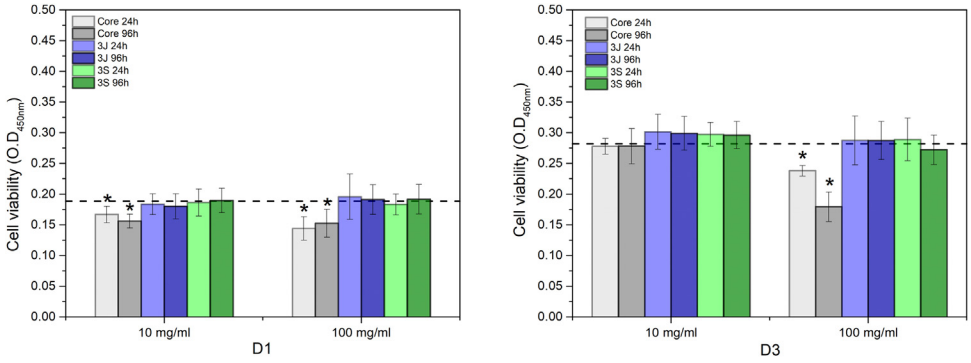

Fig. 8 – Cell viability of the MG-63 cells after 1 day (D1) and 3 days (D3) incubated with the CCM that had been previously in contact with the core, 3J and 3S powders at 10 mg/ml and 100 mg/ml for 24 h and 96 h. * means a significant difference ($p < 0.05$) compared to the control.

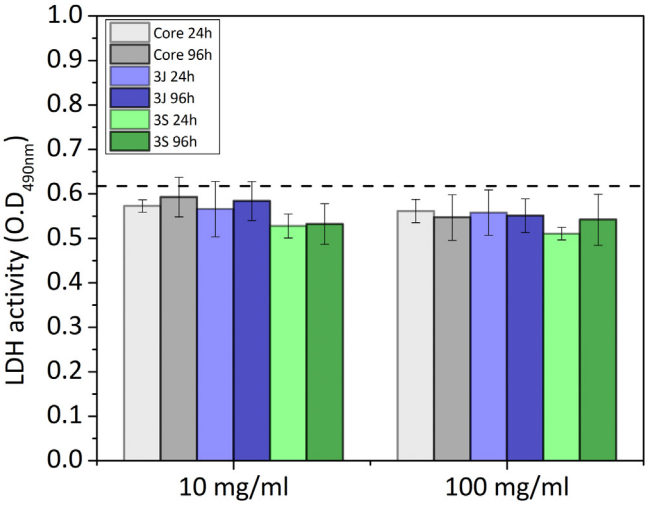

Fig. 9 – LDH activity of the MG-63 cells after 3 days incubated with the CCM that had previously been in contact with the core, 3J and 3S powders at 10 mg/ml and 100 mg/ml for 24 h and 96 h.

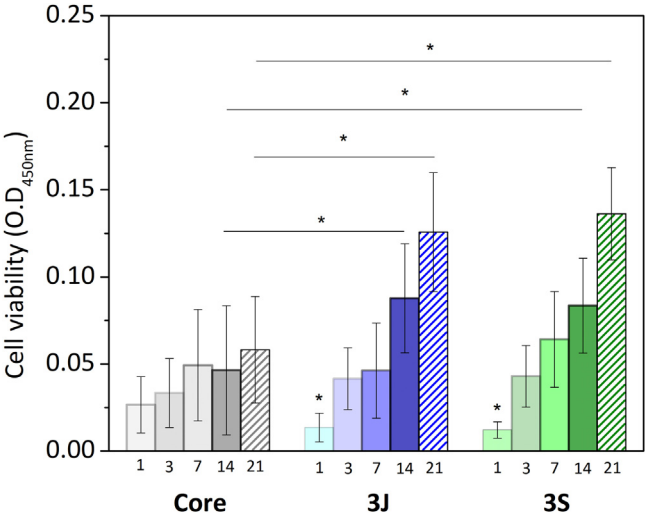

Fig. 10 – Cell viability of the MG-63 cells in contact with the core and scaffolds 3J and 3S between 1 and 21 days. * means a significant difference ($p < 0.05$) compared to the core.

to the formation of new cell colonies. Some cells were still round-shaped, but others had partially expanded.

Fig. 13 illustrates the SEM images. At 3 days, some cells were observed on the core's surface (Fig. 13A), but more cells were noted on the surface of scaffolds 3J (Fig. 13B) and 3S (Fig. 13C). The cells observed on the surface of scaffold 3J started to expand (dotted line), while those cells on the surface of scaffold 3S were more elongated. After 14 days on scaffolds 3J (Fig. 13E) and 3S (Fig. 13F), a dense and large layer of cells covering the entire scaffold surface formed, which became denser after 21 days (Fig. 13H–I). In contrast, on the core surface, a layer of cells began to form after 21 days (Fig. 13G).

Discussion

In order to implement new strategies to cover bone-implant demands, this research work proposes a new combination of ceramic materials. These new multilayer ceramic scaffolds, doped with iron, strontium and magnesium in two different configurations, allowed to cover the following properties in a single scaffold: mechanical strength, porosity, bioactivity, and good interaction with cells.

First, the core of the scaffold was obtained and the most outstanding characteristic was the mechanical resistance. The compressive strength of the scaffold's core, constituted mainly by calcium pyrophosphate (Fig. 1), was close to the lower trabecular bone strength limit reported as 1.5–7.5 MPa (Fig. 3) depending on the body area [25]. The lithium added in the core formulation contributes to this mechanical strength, as was reported in another study with TCP materials [26].

As regards *in vitro* bioactivity, it has been previously found that this scaffold did not present *in vitro* bioactivity due to the inhibitory effect of pyrophosphate [18,27]. In fact, the silicon added to promote ion exchange and generate nucleation points was not enough to overcome the effect of pyrophosphate.

Please cite this article in press as: N.A. Mata, et al., Effect of Sr, Mg and Fe substitution on the physico-chemical and biological properties of Si—Ca—P multilayer scaffolds, Bol. Soc. Esp. Cerám. Vidr. (2021), https://doi.org/10.1016/j.bsecv.2021.11.005

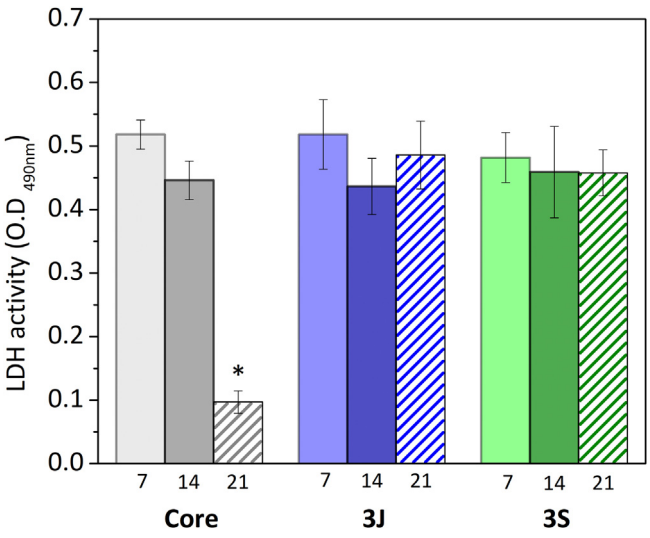

Fig. 11 – LDH activity of the MG-63 cells in contact with the core and scaffolds 3J and 3S after 7, 14 and 21 days. * means a significant difference ($p < 0.05$) compared to the control.

However, the present study demonstrates its behavior in the presence of cells. By an indirect cell culture assay, the ions released by the core lowered the pH (Fig. 6), which acidified the medium and, therefore, decreased cell viability (Fig. 8). The most significant ionic variation in the core was the release of phosphorus, lithium, and silicon (Fig. 7). The release of lithium and silicon to the medium created attraction points for the protons of water molecules, which led to the release of OH^- that was unable to explain the drop in pH. This suggests that medium acidification resulted from the breaking of P—O—P bonds due to the attack of water molecules, which caused $2PO_4^{3-} + 2H^+$ to form and, consequently, the release of H^+ protons to the medium. Due to the excessive release of phosphorus, a drop in pH was the predominant effect. Despite diminished cell viability, no significant cytotoxic effects were evidenced in the indirect assay in relation to the control (Fig. 9).

Although cell viability remained practically constant over time in the direct assay (Fig. 10), a drop in the number of cells was observed after 21 days (Fig. 11). The viability and cytotoxicity assays complement each other. The first one only shows the mitochondrial activity of the cells in the material and the second one effectively demonstrates how many cells remain in contact with the material. In this case, the lower amount of cells observed after 21 days, indicates the consequences of prolonged medium acidification.

In addition, nor were cell adhesion and proliferation on the surface favored (Figs. 12 and 13). This behavior has also been reported by Banerjee et al., who compared the TCP surface and attributed this behavior to the interface's instability and to lack of apatite precipitates, which beneficially interact with cells [28].

The core's negative response in the presence of cells differed from that indicated by other studies that have reported calcium pyrophosphate as a biocompatible material [29–31]. However, when comparing other studies to the present work, we found that none of them analyzed pH variations in cell culture medium over time, and the material concentrations were low (1000 μg/ml) compared to those herein employed [29,31]. In addition, calcium pyrophosphates reported in other research works were prepared by different methods. The materials obtained by the sol-gel process, as in this work, were characterized by a large specific surface area and were, therefore, more reactive [32]. In any case, material acidification, which triggers reduced cell activity, is an effect that can take place thanks to the static conditions in the study, but in dynamic conditions, *in vivo*, this might not be an inconvenience. Calcium pyrophosphate occurs naturally in the organism and is a bone mineralization regulator together with the action of other enzymes [33].

Despite the drawbacks presented by the core in the cellular assays *in vitro*, it served as a support for the external coatings with a higher percentage of silicon and dopant ions. The scaffolds' mechanical strength doubled after coatings (Fig. 3) and overcame the lower compressive strength limit reported for trabecular bone [25]. Consequently, porosity decreased by approximately 25% in relation to the core due to the pore plugging caused by the more viscous coatings (Fig. 3). The SEM images illustrate the presence of coating layers. By analyzing surface areas by EDX, the presence of dopant ions was confirmed (Fig. 2).

Although the coatings of scaffolds 3J and 3S were constituted by the same ions, the sintering thermal treatments

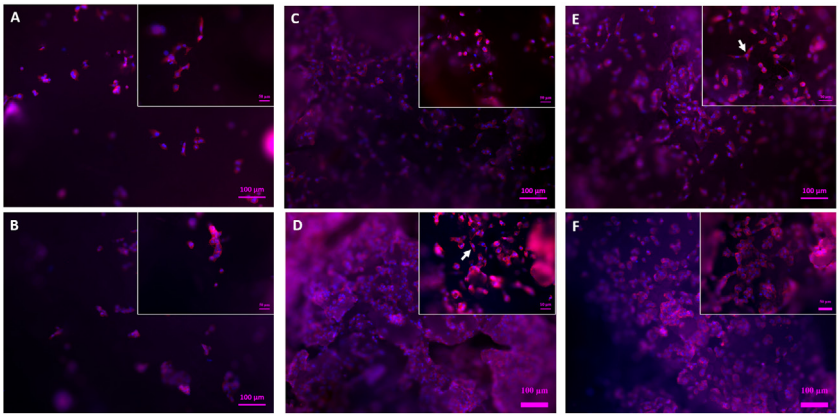

Fig. 12 – Fluorescence staining of the nuclei (blue) and cytoskeleton (red) of the MG-63 cells on the surface of the core (A, B), and scaffolds 3J (C, D) and 3S (E, F) after 3 and 7 days.

Please cite this article in press as: N.A. Mata, et al., Effect of Sr, Mg and Fe substitution on the physico-chemical and biological properties of Si—Ca—P multilayer scaffolds, Bol. Soc. Esp. Cerám. Vidr. (2021), https://doi.org/10.1016/j.bsecv.2021.11.005

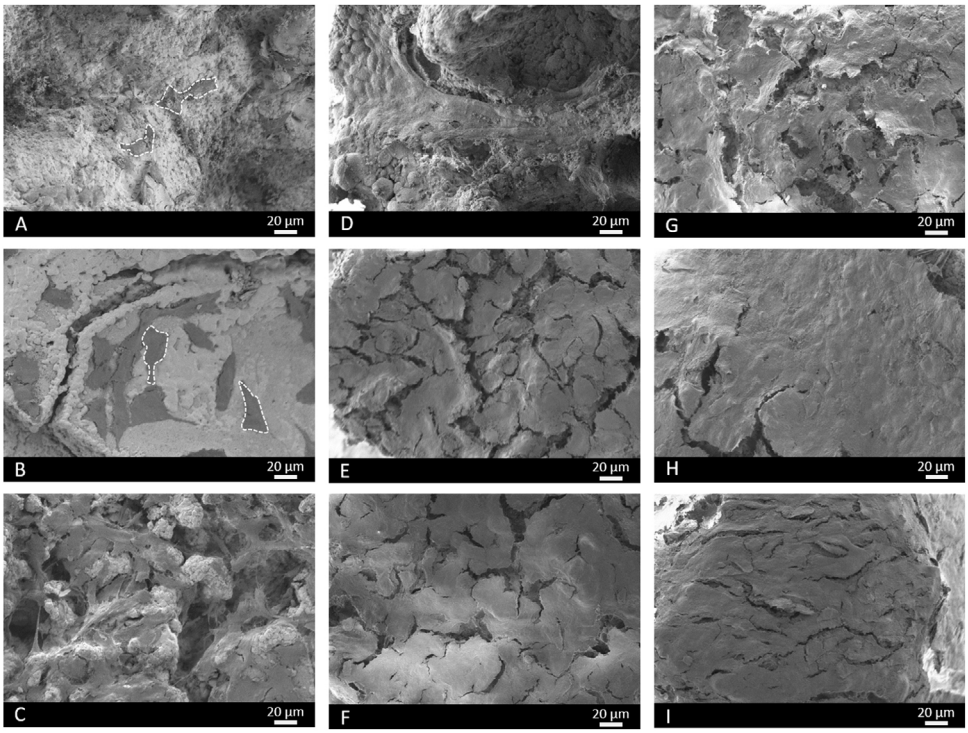

Fig. 13 – SEM images of the core (A, D, G) and scaffolds 3J (B, E, H) and 3S (C, F, I) after 3 (A–C), 14 (D–F) and 21 days (G–I) of immersion in the CCM with MG-63 cells.

differed. Scaffolds 3J were resintered after coating, while scaffolds 3S had three different coatings and were sintered 3 more times. These processes allowed the dopant ions to be distributed differently in each scaffold as evidenced by XRD (Fig. 1). The first noteworthy behavior was the shift in peak at 29.57°, which corresponded to calcium pyrophosphate. This meant that a distortion occurred in the crystal lattice from substituting calcium ions for smaller ions that tensed the lattice. The ionic radius of Ca^{2+} was 1.00 Å [34] and that of dopant ions Sr^{2+} was 1.18 Å [34], with 0.72 Å for Mg^{2+} [34] and 0.64 Å for Fe^{3+} [35]. This suggests that ions smaller than calcium moved to the crystal lattice, such as magnesium, because the magnesium-substituted calcium pyrophosphate ($Mg_2P_2O_7$) was identified. This shift has also been reported by Kim et al. when doping calcium pyrophosphate with 1, 3 and 5 wt% Mg^{2+} [34].

Another change observed by XRD was the tendency to form phases substituted by ions smaller than calcium such as iron and magnesium. Sintering processes in the presence of dopant ions promoted the conversion of calcium pyrophosphate into TCP.

Due to the presence of a higher silicon content in external coatings, new combined phases were formed, such as silica, strontium silicate and non-stoichiometric silicates with magnesium, iron and calcium. The combined phases with iron and magnesium showed that the competitive behavior of both ions was smaller in size than calcium, while strontium was bigger and formed an independent phase. Although a small amount was identified from the strontium silicate phase, it was assumed that the remaining species formed an amorphous phase. The peak corresponding to silica increased in scaffolds 3S compared to scaffolds 3J because having three coatings presented 3-fold the amount of silicon.

Although scaffolds 3J and 3S had the same phases, as expected because both contained the same ions, the proportion of each phase differed. With each sintering process, calcium pyrophosphate decreased and non-stoichiometric TCP increased with different ions. It is even observed that TCP-Mg phase was the main phase in relation to the TCP-Fe phase confirming that magnesium ions tended to stabilize TCP, as reported by Torres et al. and Zhou et al. [36,37].

The lithium ions introduced into the core formed the $Li(PO_3)$ phase and were introduced into the calcium pyrophosphate lattice given the peak shift. Due to coatings and heat treatments, these lithium ions subsequently formed part of the diffusion processes that led to the TCP-Li phase in scaffold 3S. In the 3J scaffold this phase was not observed since having only one sintering process compared to the 3S scaffold, the reduced diffusion did not allow the formation of any crystalline phase. Therefore, the lithium remained forming amorphous phase or within the crystalline lattice of the calcium pyrophosphate. All these changes between scaffolds 3S and 3J are summarized insofar as scaffolds 3S formed more TCP phases and possessed a larger amount of silicon.

The *in vitro* bioactivity evaluation showed that scaffolds 3J exhibited bioactive behavior at 21 days, while scaffold 3S did so at 3 days (Fig. 4), due to the presence of precipitates with a typical apatite morphology [38,39]. On the first testing days, dissolution of coating layers was observed on the surface of scaffolds 3J, which was also evidenced by the release of phosphorus to SBF (Fig. 5) and calcium adsorption on the scaffold surface. After 21 days, when silicon and strontium were

Please cite this article in press as: N.A. Mata, et al., Effect of Sr, Mg and Fe substitution on the physico-chemical and biological properties of Si—Ca—P multilayer scaffolds, Bol. Soc. Esp. Cerám. Vidr. (2021), https://doi.org/10.1016/j.bsecv.2021.11.005

released, apatite precipitation occurred. Conversely, scaffold 3S released silicon and strontium on day 3, which led to the adsorption of calcium and phosphorus from SBF to apatite precipitate.

Due to the number of crystalline and non-crystalline phases in scaffolds, establishing a mechanism to explain the bioactivity is complicated. However, due to the amount of silicon in external coatings and the formation of new non-stoichiometric TCP phases, bioactivity could be explained by the mechanisms already proposed by Hench for bioactive glass ceramics and calcium phosphates [40,41]. Scaffolds 3S had more silicon and its release on day 3 created nucleation points for apatite precipitates. This confirmed the rapid decrease of calcium and phosphorus on day 3. Strontium was released simultaneously with silicon, which could be related to either the dissolution of the strontium silicate phase identified by XRD or the amorphous phase between silicon and strontium. The bioactivity of scaffolds 3S could also be due to the TCP phases. It is known that given its negative surface, TCP attracts Ca^{2+} ions from SBF and creates a nucleation point for apatite precipitates [28,41]. Zhou et al. have confirmed that the TCP-Mg surface is more negative than TCP and can, therefore, more strongly attract ions, and can even adsorb magnesium ions from SBF, which occurred at 21 days [37]. Both effects provided scaffolds 3S a significant bioactive behavior. In contrast, as scaffolds 3J did not have many silicon and TCP phases, the mechanisms were delayed until 21 days when silicon was released. Moreover, it also had larger amounts of calcium pyrophosphate and magnesium pyrophosphate phases in the inner part, which are known to inhibit apatite precipitation *in vitro* due to the P-O-P bond of the pyrophosphate group [18,27].

Regarding the interaction between scaffolds 3J and 3S and MG-63 cells, the ions released by the materials in the indirect assay slightly increased cell viability after 3 days (Fig. 8). The analysis of the ionic concentrations indicated that the release of silicon could be primarily responsible for the slight increase in viability as the dopant ions of strontium, iron and magnesium were not significantly released during the study time, except for the extracts of scaffolds 3J at 100 mg/ml (Fig. 7). Silicon plays a key role in cellular response. Han et al. have demonstrated that silicon enhances cell proliferation, differentiation and mineralization [42]. This could be another reason for the better performance of scaffolds 3J and 3S compared to the core. Xing et al. utilized the benefits of silicon and strontium to demonstrate the synergistic effect when combining both ions in a single structure, and they observed the stimulation of cell proliferation and osteogenic differentiation [43]. The release of silicon is closely related to the presence of strontium, as demonstrated by Yin et al. when doping boron bioglasses with strontium, these authors noted a faster release of silicon and the increased proliferation of MG-63 cells [44]. This could explain the joint release of silicon and strontium herein evidenced.

The effect of dopants and their arrangement on viability were studied by the direct assay. When cells were evaluated directly on the scaffolds surface, cell viability increased with time, and increased by more than 100% compared to the core after 21 days (Fig. 10). In relation to cell morphology, cell proliferation on the surfaces of scaffolds 3J and 3S was greater than on the core's surface (Figs. 12 and 13). The cell colonies in the core were initially more agglomerated, while cells were more spread out and adhered to the surface of scaffolds 3J and 3S. The dense and continuous layers of the cells that formed on the surface of scaffolds 3J and 3S after 14 days demonstrated not only the positive effect of ions on the surface that had not yet been released, but also the influence of the silicon released to the medium.

The dopant ions herein used had positive effects on cellular response. Strontium and iron ions possess angiogenic, osteogenic and antibacterial properties, and strontium is widely used to treat osteoporosis [19,22,45]. Magnesium influences the activity of osteoblasts and osteoclasts [19]. To our knowledge, however, there is no material that combines strontium, iron and magnesium ions. Some studies have reported the combination of two of these ions. For example, Kim et al. have demonstrated that calcium pyrophosphate doped with strontium and magnesium is a biocompatible material [34]. The same has been observed by Singh et al. and Vahabzadeh et al. when doping tricalcium phosphate with iron ions [46,47]. Tricalcium phosphate has been doped with magnesium at different concentrations, and Gu et al. have reported how magnesium not only increases cell proliferation, but also improves cell morphology and viability [48]. During the cell culture assays in the above study, the authors observed how magnesium and calcium ions decreased in the medium over time (which was also the case in our work), and they attributed this behavior to apatite deposition and mineralization. Although no release of magnesium ions was seen, these ions may enhance cell adhesion by influencing the interaction with integrin that acts as an adhesion protein [24,49]. Lithium was also one of the ions released mainly by the core. This ion has long since been used to treat mental disorders but has recently been employed to improve compressive strength and has positive effects on angiogenesis [26,50]. However, the influence of this ion on the cells that came into contact with the core was not observed in our work due to the effect of lowering the pH, while the release of lithium in scaffolds 3J and 3S could enhance the effect of the other ions.

It was generally found that the behavior of the cells that came into contact with scaffolds 3J and 3S was similar, with no direct influence of ion arrangement on the interaction with cells. On the contrary, the ion arrangement affected crystalline phases and their *in vitro* bioactivity behavior.

It is possible to consider that the core, being the common base of the scaffolds 3J and 3S, may cause cytotoxic effects when the coatings dissolve. However, the indirect cell assays revealed that the core's acidification effect disappeared after crushing the scaffolds and mixing the core material with outer coatings. This could be due to the decrease in the calcium pyrophosphate phase which, as sintering proceeded was transformed into TCP phases, and would mean that the amount of calcium pyrophosphate would not be sufficient to cause acidification. As previously mentioned, acidification is a negative effect in static *in vitro* tests, but should not be a drawback *in vivo* because pyrophosphate is a natural bone mineralization regulator.

Please cite this article in press as: N.A. Mata, et al., Effect of Sr, Mg and Fe substitution on the physico-chemical and biological properties of Si—Ca—P multilayer scaffolds, Bol. Soc. Esp. Cerám. Vidr. (2021), https://doi.org/10.1016/j.bsecv.2021.11.005

Conclusions

In this research work, multilayer ceramic scaffolds were developed as a future alternative for bone tissue engineering applications. The scaffold's core, constituted mainly by calcium pyrophosphate, did not show a good cellular response, but its structure exhibiting mechanical resistance served as a support to apply the external coatings constituted mainly by calcium and silicon, and doped with iron, strontium and magnesium ions (3J and 3S). Cell viability in scaffolds 3J and 3S increased by more than 100% *vs.* the core, and cell proliferation and adhesion improved by the formation of a dense layer of cells that covered the entire surface after 21 days. In cellular terms, there was no significant difference between the arrangement of dopant ions. In bioactivity terms, however, scaffolds 3S (ions in separate coatings) presented bioactivity at 3 days, while scaffolds 3J (ions in the same coating) did so at 21 days, which was attributed to the larger amount of silicon in the external coatings.

Conflict of interest

None.

Acknowledgements

Ph.D. student Nayarit A. Mata was funded by a grant from the Generalitat Valenciana with reference GRISOLIAP/2018/037 and pre-doctoral mobility co-financed by the European Social Fund and the Generalitat Valenciana with reference BEFPI/2021/056. This publication is part of the Grant PID2020-116693RB-C21 funded by MCIN/AEI/10.13039/501100011033.

REFERENCES

[1] P. Verma, V. Verma, Concepts of tissue engineering, Anim. Biotechnol. (2020) 295–307, http://dx.doi.org/10.1016/B978-0-12-811710-1.00013-6, Elsevier.
[2] A. Przekora, The summary of the most important cell-biomaterial interactions that need to be considered during in vitro biocompatibility testing of bone scaffolds for tissue engineering applications, Mater. Sci. Eng. C 97 (2019) 1036–1051, http://dx.doi.org/10.1016/j.msec.2019.01.061.
[3] J.J. Li, D.L. Kaplan, H. Zreiqat, Scaffold-based regeneration of skeletal tissues to meet clinical challenges, J. Mater. Chem. B 2 (42) (2014) 7272–7306, http://dx.doi.org/10.1039/c4tb01073f.
[4] H. Qu, H. Fu, Z. Han, Y. Sun, Biomaterials for bone tissue engineering scaffolds: a review, RSC Adv. 9 (45) (2019) 26252–26262, http://dx.doi.org/10.1039/c9ra05214c.
[5] Pearlin, S. Nayak, G. Manivasagam, D. Sen, Progress of regenerative therapy in orthopedics, Curr. Osteoporos. Rep. 16 (2) (2018) 169–181, http://dx.doi.org/10.1007/s11914-018-0428-x.
[6] M.P. Murphy, M.R. Borrelli, D.T. Montoro, M.T. Longaker, D.C. Wan, Skeletal tissue engineering, Princ. Tissue Eng. (2020) 1007–1021, http://dx.doi.org/10.1016/B978-0-12-818422-6.00057-5, Elsevier.
[7] S.V. Dorozhkin, Current state of bioceramics, J. Ceram. Sci. Technol. 9 (4) (2018) 353–370, http://dx.doi.org/10.4416/JCST2018-00026.
[8] A. Wubneh, E.K. Tsekoura, C. Ayranci, H. Uludağ, Current state of fabrication technologies and materials for bone tissue engineering, Acta Biomater. 80 (2018) 1–30, http://dx.doi.org/10.1016/j.actbio.2018.09.031.
[9] W. Wang, K.W.K. Yeung, Bone grafts and biomaterials substitutes for bone defect repair: a review, Bioact. Mater. 2 (4) (2017) 224–247, http://dx.doi.org/10.1016/j.bioactmat.2017.05.007.
[10] Y. Yang, Y. Kang, M. Sen, S. Park, Biomaterials in tissue engineering, Biomater. Tissue Eng. Appl. A Rev. Past Futur. Trends (2011) 1–564, http://dx.doi.org/10.1007/978-3-7091-0385-2, Springer-Verlag.
[11] G.M. Raghavendra, K. Varaprasad, T. Jayaramudu, Biomaterials: design, development and biomedical applications, Nanotechnol. Appl. Tissue Eng. (2015) 21–44, http://dx.doi.org/10.1016/B978-0-323-32889-0.00002-9, Elsevier.
[12] N. Eliaz, N. Metoki, Calcium phosphate bioceramics: a review of their history, structure, properties, coating technologies and biomedical applications, Materials 10 (4) (2017), http://dx.doi.org/10.3390/ma10040334.
[13] I. Denry, L.T. Kuhn, Design and characterization of calcium phosphate ceramic scaffolds for bone tissue engineering, Dent. Mater. 32 (1) (2016) 43–53, http://dx.doi.org/10.1016/j.dental.2015.09.008.
[14] S. Bose, M. Roy, A. Bandyopadhyay, Recent advances in bone tissue engineering scaffolds, Trends Biotechnol., 30(10) 546–554, doi:10.1016/j.tibtech.2012.07.005.
[15] P. Ros-Tárraga, N.A. Mata, Á. Murciano, P. Velasquez, P.N. De Aza, Multilayer ceramic materials: a method to link bioactivity and durability, Ceram. Int. 45 (17) (2019) 23611–23618, http://dx.doi.org/10.1016/j.ceramint.2019.08.072.
[16] N.A. Mata, P. Ros-Tárraga, P. Velasquez, A. Murciano, P.N. De Aza, Synthesis and characterization of 3D multilayer porous Si–Ca–P scaffolds doped with Sr ions to modulate in vitro bioactivity, Ceram. Int. 46 (1) (2020) 968–977, http://dx.doi.org/10.1016/j.ceramint.2019.09.058.
[17] N.A. Mata, P. Ros-Tárraga, P. Velasquez, A. Murciano, P.N. De Aza, New iron-doped multilayer ceramic scaffold with noncontinuous bioactive behavior, Ceram. Int. 46 (10) (2020) 16388–16396, http://dx.doi.org/10.1016/j.ceramint.2020.03.198.
[18] N.A. Mata, P. Velasquez, A. Murciano, P.N. De Aza, Multilayer Mg-pyrophosphate glass ceramic with discontinuous bioactivity. Physicochemical characterization, Ceram. Int. 47 (10) (2021) 14612–14620, http://dx.doi.org/10.1016/j.ceramint.2021.02.044.
[19] V.M. Schatkoski, et al., Current advances concerning the most cited metal ions doped bioceramics and silicate-based bioactive glasses for bone tissue engineering, Ceram. Int. 47 (3) (2021) 2999–3012, http://dx.doi.org/10.1016/j.ceramint.2020.09.213.
[20] S. Meininger, et al., Effect of strontium substitution on the material properties and osteogenic potential of 3D powder printed magnesium phosphate scaffolds, Mater. Sci. Eng. C 98 (2019) 1145–1158, http://dx.doi.org/10.1016/j.msec.2019.01.053.
[21] D. Ke, S. Tarafder, S. Vahabzadeh, S. Bose, Effects of MgO, ZnO, SrO, and SiO_2 in tricalcium phosphate scaffolds on in vitro gene expression and in vivo osteogenesis, Mater. Sci. Eng. C 96 (2019) 10–19, http://dx.doi.org/10.1016/j.msec.2018.10.073.

Please cite this article in press as: N.A. Mata, et al., Effect of Sr, Mg and Fe substitution on the physico-chemical and biological properties of Si—Ca—P multilayer scaffolds, Bol. Soc. Esp. Cerám. Vidr. (2021), https://doi.org/10.1016/j.bsecv.2021.11.005

[22] M. S. Araujo, A. C. Silva, B. Cabal, J. F. Bartolomé, and S. Mello-Castanho, In vitro bioactivity and antibacterial capacity of 45S5 Bioglass®-based compositions containing alumina and strontium, J. Mater. Res. Technol., 13, 154–161. doi:10.1016/j.jmrt.2021.04.053.
[23] S.M. Rabiee, N. Nazparvar, M. Azizian, D. Vashaee, L. Tayebi, Effect of ion substitution on properties of bioactive glasses: a review, Ceram. Int. 41 (6) (2015) 7241–7251, http://dx.doi.org/10.1016/j.ceramint.2015.02.140.
[24] A. Hoppe, N.S. Güldal, A.R. Boccaccini, A review of the biological response to ionic dissolution products from bioactive glasses and glass-ceramics, Biomaterials 32 (11) (2011) 2757–2774, http://dx.doi.org/10.1016/j.biomaterials.2011.01.004.
[25] G. Kaur, et al., Mechanical properties of bioactive glasses, ceramics, glass-ceramics and composites: state-of-the-art review and future challenges, Mater. Sci. Eng. C 104 (2019), http://dx.doi.org/10.1016/j.msec.2019.109895, 109895.
[26] C.Q. Zhao, et al., Doping lithium element to enhance compressive strength of β-TCP scaffolds manufactured by 3D printing for bone tissue engineering, J. Alloys Compd. 814 (2020), http://dx.doi.org/10.1016/j.jallcom.2019.152327.
[27] H. Fleisch, S. Bisaz, Mechanism of calcification: inhibitory role of pyrophosphate, Nature 195 (4844) (1962) 911, http://dx.doi.org/10.1038/195911a0.
[28] S.S. Banerjee, A. Bandyopadhyay, S. Bose, Biphasic resorbable calcium phosphate ceramic for bone implants and local alendronate delivery, Adv. Eng. Mater. 12 (5) (2010) 148–155, http://dx.doi.org/10.1002/adem.200980072.
[29] E. Alsubhe, et al., Analysis of the osteogenic and mechanical characteristics of iron (Fe^{2+}/Fe^{3+})-doped β-calcium pyrophosphate, Mater. Sci. Eng. C 115 (2020) 111053, http://dx.doi.org/10.1016/j.msec.2020.111053.
[30] S.R. Vasant, M.J. Joshi, A review on calcium pyrophosphate and other related phosphate nano bio-materials and their applications, Rev. Adv. Mater. Sci. 49 (1) (2017) 44–57.
[31] A.D. Anastasiou, et al., β-Pyrophosphate: a potential biomaterial for dental applications, Mater. Sci. Eng. C 75 (2017) 885–894, http://dx.doi.org/10.1016/j.msec.2017.02.116.
[32] G.J. Owens, et al., Sol–gel based materials for biomedical applications, Prog. Mater. Sci. 77 (2016) 1–79, http://dx.doi.org/10.1016/j.pmatsci.2015.12.001.
[33] I.R. Orriss, T.R. Arnett, R.G.G. Russell, Pyrophosphate: a key inhibitor of mineralisation, Curr. Opin. Pharmacol. 28 (2016) 57–68, http://dx.doi.org/10.1016/j.coph.2016.03.003.
[34] D.W. Kim, J.S. An, I.S. Cho, Effects of Mg and Sr co-addition on the densification and biocompatible properties of calcium pyrophosphate, Ceram. Int. 44 (8) (2018) 9689–9695, http://dx.doi.org/10.1016/j.ceramint.2018.02.198.
[35] I. Ullah, et al., Simultaneous co-substitution of Sr^{2+}/Fe^{3+} in hydroxyapatite nanoparticles for potential biomedical applications, Ceram. Int. 44 (17) (2018) 21338–21348, http://dx.doi.org/10.1016/j.ceramint.2018.08.187.
[36] P.M.C. Torres, et al., Influence of Mg-doping, calcium pyrophosphate impurities and cooling rate on the allotropic α↔β-tricalcium phosphate phase transformations, J. Eur. Ceram. Soc. 36 (3) (2016) 817–827, http://dx.doi.org/10.1016/j.jeurceramsoc.2015.09.037.
[37] H. Zhou, et al., Synthesis of β-TCP and CPP containing biphasic calcium phosphates by a robust technique, Ceram. Int. 42 (9) (2016) 11032–11038, http://dx.doi.org/10.1016/j.ceramint.2016.03.246.
[38] F.E. Ciraldo, et al., Fabrication and characterization of Ag- and Ga-doped mesoporous glass-coated scaffolds based on natural marine sponges with improved mechanical properties, J. Biomed. Mater. Res. – Part A (2020) 1–19, http://dx.doi.org/10.1002/jbm.a.37123.
[39] M. Arango-Ospina, K. Lasch, J. Weidinger, A.R. Boccaccini, Manuka Honey and Zein coatings impart bioactive glass bone tissue scaffolds antibacterial properties and superior mechanical properties, Front. Mater. 7 (2021) 1–12, http://dx.doi.org/10.3389/fmats.2020.610889.
[40] L.L. Hench, Bioceramics: from concept to clinic. J. Am. Ceram. Soc. 72 (1993) 93–98. J. Am. Ceram. Soc., 74 (1991) 1487–1510.
[41] H.M. Kim, T. Himeno, T. Kokubo, T. Nakamura, Process and kinetics of bonelike apatite formation on sintered hydroxyapatite in a simulated body fluid, Biomaterials 26 (21) (2005) 4366–4373, http://dx.doi.org/10.1016/j.biomaterials.2004.11.022.
[42] P. Han, C. Wu, Y. Xiao, The effect of silicate ions on proliferation, osteogenic differentiation and cell signalling pathways (WNT and SHH) of bone marrow stromal cells, Biomater. Sci. 1 (4) (2013) 379–392, http://dx.doi.org/10.1039/c2bm00108j.
[43] M. Xing, X. Wang, E. Wang, L. Gao, J. Chang, Bone tissue engineering strategy based on the synergistic effects of silicon and strontium ions, Acta Biomater. 72 (2018) 381–395, http://dx.doi.org/10.1016/j.actbio.2018.03.051.
[44] H. Yin, et al., Fabrication and characterization of strontium-doped borate-based bioactive glass scaffolds for bone tissue engineering, J. Alloys Compd. 743 (2018) 564–569, http://dx.doi.org/10.1016/j.jallcom.2018.01.099.
[45] S.H. Lin, W.J. Zhang, X.Q. Jiang, Applications of bioactive ions in bone regeneration, Chin. J. Dent. Res. 22 (2) (2019) 93–104, http://dx.doi.org/10.3290/j.cjdr.a42513.
[46] R.K. Singh, M. Srivastava, N.K. Prasad, S. Awasthi, A. Dhayalan, S. Kannan, Iron doped β-tricalcium phosphate: synthesis, characterization, hyperthermia effect, biocompatibility and mechanical evaluation, Mater. Sci. Eng. C 78 (2017) 715–726, http://dx.doi.org/10.1016/j.msec.2017.04.130.
[47] S. Vahabzadeh, S. Bose, Effects of iron on physical and mechanical properties, and osteoblast cell interaction in β-tricalcium phosphate, Ann. Biomed. Eng. 45 (3) (2017) 819–828, http://dx.doi.org/10.1007/s10439-016-1724-1.
[48] Y. Gu, J. Zhang, X. Zhang, G. Liang, T. Xu, W. Niu, Three-dimensional printed Mg-doped β-TCP bone tissue engineering scaffolds: effects of magnesium ion concentration on osteogenesis and angiogenesis in vitro, Tissue Eng. Regen. Med. 16 (4) (2019) 415–429, http://dx.doi.org/10.1007/s13770-019-00192-0.
[49] H. Zreiqat, et al., Mechanisms of magnesium-stimulated adhesion of osteoblastic cells to commonly used orthopaedic implants, J. Biomed. Mater. Res. 62 (2) (2002) 175–184, http://dx.doi.org/10.1002/jbm.10270.
[50] L. Liu, et al., Lithium-containing biomaterials stimulate bone marrow stromal cell-derived exosomal miR-130a secretion to promote angiogenesis, Biomaterials 192 (2019) 523–536, http://dx.doi.org/10.1016/j.biomaterials.2018.11.007.

Please cite this article in press as: N.A. Mata, et al., Effect of Sr, Mg and Fe substitution on the physico-chemical and biological properties of Si—Ca—P multilayer scaffolds, Bol. Soc. Esp. Cerám. Vidr. (2021), https://doi.org/10.1016/j.bsecv.2021.11.005